Friction **10**(12): 1985–1999 (2022)
https://doi.org/10.1007/s40544-021-0560-y
ISSN 2223-7690
CN 10-1237/TH
RESEARCH ARTICLE

Fabrication of high-stability Ni-PSF@PAO40 microcapsules and their lubricating properties in polyamide 6

Wenli ZHANG[1,2], Xiaowen QI[1,3,*], Xiao YANG[1,2], Yu DONG[4], Bingli FAN[1,3,*], Lei LIANG[5]

[1] *School of Mechanical Engineering, Yanshan University, Qinhuangdao 066004, China*

[2] *Key Laboratory of Self-Lubricating Spherical Plain Bearing technology of Hebei Province, Yanshan University, Qinhuangdao 066004, China*

[3] *Aviation Key Laboratory of Science and Technology on Generic Technology of Self-Lubricating Spherical Plain Bearing, Yanshan University, Qinhuangdao 066004, China*

[4] *School of Civil and Mechanical Engineering, Curtin University, Perth, WA 6845, Australia*

[5] *Shanghai Research Institute of Synthetic Resins Co., Ltd., Shanghai 201702, China*

Received: 24 July 2021 / Revised: 30 August 2021 / Accepted: 30 September 2021

Abstract: Novel Ni-PSF@PAO40 microcapsules (NPPMS) with high stability were prepared by using a combined processing method of electroless nickel plating and solvent volatilization. The results indicate that Ni is completely assembled on the surfaces of PSF/PAO40 microcapsules with the encapsulation capacity of NPPMS achieved at 50%. Organic solvents immersion shows that NPPMS have an excellent chemical stability. Macro thermal stability tests reveal that the softening temperature of NPPMS is increased up to over 400 °C while it becomes lower than 200 °C for PSF/PAO40 microcapsules. Furthermore, NPPMS were embedded into polyamide 6 (PA6) to prepare PA6/NPPMS composites. The cross-sectional morphology shows that NPPMS are intact in PA6 matrices. The microhardness of PA6 is effectively improved with the incorporation of NPPMS. As compared with neat PA6, the coefficient of friction (COF) for PA6/NPPMS composites with 10% NPPMS could be reduced by 87.7% (from 0.49 to 0.06) and the wear rate could be decreased by 96.8% (from 1.29×10^{-5} to 4.15×10^{-7} mm^3/(N·m)). Further studies confirmed that increasing test loads and test temperatures was beneficial to improve the lubrication performance of NPPMS despite the opposite trend occurred when increasing the sliding speeds. It has been demonstrated that synergistic effects between PAO40 and Ni layer play an important role in improving the tribological properties of PA6. Therefore, NPPMS significantly improve the ability of microcapsules to resist a harsh environment, which has important scientific significance for expanding the use of microcapsules more practically in self-lubricating composites.

Keywords: microcapsules; electroless nickel; high temperature resistant; polyamide 6 (PA6); friction and wear

1 Introduction

In recent years, microcontainers carrying lubricating oils have attracted great interests to the wide research and industrial communities because they can be embedded into polymer matrices to form a new type of self-lubricating composites with ultra-low coefficient of friction (COF) and wear rate. Hollow microspheres [1], porous microspheres [2], metal-organic frameworks (MOFs) [3], and microcapsules [4] are usually used as the microcontainers for storing lubricating oil to achieve automatic release of lubrication in polymer matrices. Among them, microcapsules as a typical representative of micro-containers, have the advantages for the separation of the matrices and lubricating oil, stimulus-responsible

* Corresponding authors: Xiaowen QI, E-mail: qxw_tougao@163.com; Bingli FAN, E-mail: fanbingli@ysu.edu.cn

release (load and temperature), and controllable oil storage in order to warrant the durability and efficiency of effective lubrication.

Common preparation methods of microcapsules included solvent evaporation, interfacial polymerization, and *in-situ* polymerization, etc. [5–8]. The core materials of the microcapsules could be freely selected such as poly alpha olefin (PAO), silicone oils, liquid wax, and ionic liquid [9–13]. However, due to the limitation of preparation principles, shell materials were mostly polymers such as polysulfone (PSF), polyurethane (PU), poly(urea-formaldehyde) (PUF), poly(melamine-formaldehyde) (PMF), and polystyrene (PS) [14–19]. In order to investigate the lubricating effect of microcapsules, they were implanted into polymers to prepare polymer composites [11, 20]. For example, Zhang et al. [4] prepared PS/PAO microcapsules and incorporated them into epoxy (EP) resin and found that the COF and the wear rate of composites could be reduced to 4% (from 0.71 to 0.028) and 0.25%, respectively. Li et al. [6] prepared PU/GO hybrid wall loaded [BMIm]BF_4 microcapsules and incorporated them into EP as well. The COF and wear rate of epoxy composites were decreased by 75.4% (from 0.61 to 0.15) and 98.6 % (from 86.0×10^{-14} to 1.2×10^{-14} $m^3/(N\cdot m)$), respectively. Although microcapsules have been proven to possess excellent lubricating properties, most of previous studies [5, 6, 14, 15] on the lubrication performance of microcapsules were tested in EP matrices because the mild molding environment used for EP subjected to curing at room temperature and without pressure will not damage the fragile microcapsules. However, well-known engineering materials almost have to undergo a series of harsh environments in the molding including the dispersion of additives in organic solvents, and the process of melting and curing the matrices under continuous high temperature or high temperature/pressure. For example, in the material preparation process of polytetrafluoroethylene (PTFE)/Kevlar fabric composites, it is necessary to dilute phenolic resin with ethyl acetate to prepare impregnating liquid [21]. In the molding process of engineering thermoplastics such as polyamide (PA), polyimide (PI), polyether ether ketone (PEEK), and polyethersulfone (PES), high temperature and high pressure are usually required [22–25]. Therefore, overcoming the defects associated with poor stability of polymer shells including easy softening at high temperatures, easy damage in organic solvents, as well as poor pressure-bearing ability, has great positive impact on the further application of microcapsules.

Great efforts have been made in previous studies to improve the stability of microcapsules comprising organic/inorganic hybrid shell microcapsules, multilayer assembled microcapsules, and silica shells microcapsules using sol-gel methods [20, 26–28]. However, hybrid shell layers and multilayer-assembled layers do not form a continuously sealed inorganic skeleton while silica shell layers had the typical material demerit of high porosity, which still caused the infiltration and dissolution of organic solvents and high-temperature and high-pressure softening [29]. In addition, high-temperature stability of microcapsules should not be measured by the decomposition temperature, but is preferably based on the non-softening and rupture of microcapsules. This is because the softening temperature of polymer shells is much lower than the decomposition temperature of microcapsule components in practical applications. Therefore, it is highly suggested to develop novel microcapsules with high-stability shells.

Polymer metallization was used as a specific treatment method to obtain a metal layer on the surface of polymer matrices so that it could take the advantages of both polymers and metals. The metallized polymer surface overcame many polymeric defects along with the multifaceted characteristics of good solvent resistance, corrosion resistance, abrasion resistance, high-temperature resistance, thermal and electrical conductivity, and high mechanical strength [29–32]. Electroless plating techniques were currently one of the most widely used methods for polymer surface metallization. With the help of a reducing agent, the metal ions in the solution were preferentially reduced to the surface of catalytically active polymers such as polystyrene (PS), polymethyl methacrylate (PMMA), poly(N-isopropylacrylamide)) to generate a dense metal coating [33–35].

In this study, Ni was used as the coating metal. PSF/PAO40 microcapsules were prepared using the solvent evaporation method. In comparison, Ni-PSF shell microcapsules were prepared after surface degreasing, roughening, activation, sensitization, and

reduction. The chemical stability of Ni-PSF@PAO40 microcapsules (NPPMS) was characterized by immersing NPPMS in organic solvents such as petroleum ether, ethyl acetate, and acetone. The high-temperature resistance of NPPMS was also proved by macro thermal stability tests. Furthermore, a systematic study on tribological properties of PA6/NPPMS composites was carried out using the ball-on-disc friction tests according to microcapsule content, test load, test speed, and test temperature, which was revealed that NPPMS yielded excellent lubrication effects. The metallization of microcapsule shells solved the problem to the vulnerability of polymer shells, which was particularly useful for the application of microcapsules in a harsh environment.

2 Experimental

2.1 Materials

For the synthesis of PSF/PAO40 microcapsules, lubricant oil (PAO40) was supplied by ExxonMobil Chemical Co., Ltd., USA. Polysulfone (PSF) was purchased from Macklin Chemicals Co., Ltd., Shanghai, China. Ethanol and dichloromethane (DCM) were provided by Tianjin Kermel Chemical Reagent Co., Ltd., Tianjin, China. Gelatin was supplied by China Pharmaceutical Group Co., Ltd., Shanghai, China. For the preparation of Ni shells, detergent was supplied by Nice Group Co., Ltd., China. Potassium dichromate, sulfuric acid, and hydrochloric acid were purchased from Tianjin Kermel Chemical Reagent Co., Ltd., Tianjin, China. Sodium hydroxide, stannous chloride, nickel acetate, sodium hypophosphite monohydrate, sodium acetate, trisodium citrate, and thiourea were provided by Meryer Chemical Technology Co., Ltd., Shanghai, China. Palladium chloride and lactic acid were purchased from Bide Pharmatech Co., Ltd., Shanghai, China. All chemicals in this study were used without further modification.

2.2 Preparation of Ni-PSF@PAO40 microcapsules

PSF/PAO40 microcapsules were prepared by a solvent evaporation method, as illustrated in Fig. 1(a). PAO40 and PSF in equal mass of 0.9 g were dissolved in 40 mL DCM via magnetic stirring. Subsequently, the mixture solution was added to 300 mL gelatin solution (gelatin content: 2 wt%) using mechanical stirring at 35 °C with the rotor speed of 700 rpm. After the reaction for 3 h at 40 °C, the solvent of DCM evaporated completely and PSF/PAO40 microcapsules were obtained accordingly. Finally, prepared PSF/PAO40 microcapsules were washed with ethanol and dried at 60 °C for 12 h. Ni shell was fabricated on PSF/PAO40 microcapsule surfaces by means of electroless plating approach, as illustrated in Fig. 1(b). Firstly, the surfaces of PSF/PAO40 microcapsules were degreased. 2 g PSF/PAO40 microcapsules were added into alkaline degreasing solution including 2 g detergent, 16 g NaOH, and 200 mL deionized water and magnetically stirred at 60 °C for 1 h. After degreasing, PSF/PAO40 microcapsules were added into the coarsening solution comprising 6 g potassium dichromate, 150 mL concentrated sulfuric acid, and 200 mL deionized water, which was then treated at 70 °C for 30 minutes. Subsequently, PSF/PAO40 microcapsules were sensitized

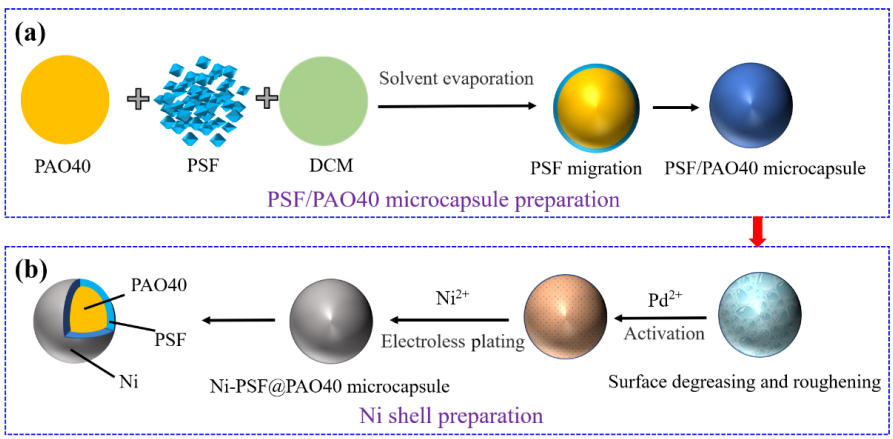

Fig. 1 Schematic diagram of NPPMS synthesis.

ultrasonically using an acid $SnCl_2$ solution consisting of 2 g $SnCl_2$, 10 mL HCl, and 200 mL deionized water at 30 °C for 10 min. Afterwards, Pd particles were deposited on the surfaces of PSF/PAO40 microcapsules for the activation. 2 g PSF/PAO40 microcapsules were added into the activation solution (i.e., 0.03 g $PdCl_2$, 2 mL HCl, and 200 mL deionized water) at 30 °C for 10 min. Finally, Ni-PSF@PAO40 microcapsules were obtained by immersing the pretreated PSF/PAO40 microcapsules in a nickel-plating solution via magnetic stirring at 70 °C for 20 min. The nickel-plating solution included 200 mL deionized water, 2 g trisodium citrate, 6 g sodium hypophosphite, 6 g nickel acetate, 6 g lactic acid, 4 g sodium acetate. Sodium hydroxide was used to control the pH level in range of 4.5–5.5. Note that prepared Ni-PSF@PAO40 microcapsules denoted NPPMS as earlier mentioned.

2.3 Preparation of PA6/NPPMS composites

The synthesized NPPMS were incorporated into PA6 for investigating the lubricating effect of NPPMS. Firstly, NPPMS with different weight fractions (i.e., 0, 5, 10, 15, and 20 wt%) were added into ethanol under ultrasonic dispersion for 10 min. Further, PA6 was added into the dispersed NPPMS solution after continuous stirring for 30 min to form the good dispersion. After suction filtration, the mixed powders were dried at 80 °C for 12 h. Subsequently, the mixed powders were placed in a graphite mold under vacuum hot press by controling the vacuum pressure being less than 10 Pa and the molding pressure of 4 MPa at the heating temperature of 260 °C for the dwell time of 30 min. The detailed vacuum hot press process in relation to the preparation of PA6/MPPMS composites was shown in Fig. 2.

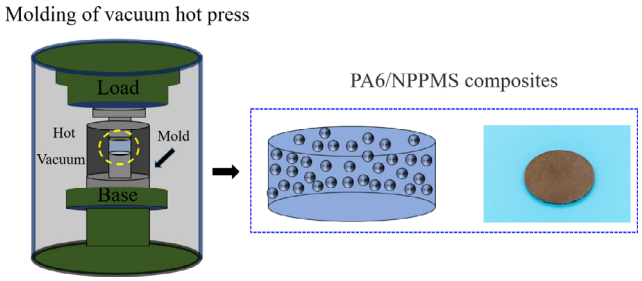

Fig. 2 Vacuum hot press process for preparing PA6/NPPMS composites.

2.4 Characterizations of NPPMS and PA6/NPPMS composites

The crystal texture of Ni-shell was analyzed by powder X-ray diffraction (XRD) using a Bruker D8 Advance X-ray diffractometer with Cu Kα radiation. The thermal stability and core content of NPPMS were evaluated using a thermogravimetric analyzer (STA449C, NETZSCH) from 30 to 70 °C at a heating rate of 10 °C/min under argon atmosphere. The morphologies of PSF/PAO40 microcapsules and NPPMS, the section morphology of PA6/NPPMS composites, Ni shells, and the wear tracks were evaluated by a scanning electron microscope (SEM) (ProX, Phenom, Holland). The chemical compositions of NPPMS and wear tracks were analyzed by an energy dispersive X-ray spectroscopy (EDS). The mechanical properties, namely microhardness and compression strength, of PA6/NPPMS composites, were determined by using a nanoindenter (Anton Paar) with 10 mN load, as well as a universal testing machine (WDW3100 KeXin, China) at a crosshead speed of 0.2 mm/min.

2.5 Tribological properties of PA6/NPPMS composites

The tribological properties of neat PA6 and PA6/NPPMS composites were carried out on a CSM-Tribotester (Anton Paar) in a reciprocating ball-on-disk mode with its testing system illustrated in Fig. 3. The bottom specimens were prepared PA6/NPPMS composites, which slid against a bearing steel ball (GCr15, ball diameter = 6 mm). The high temperature friction tests were carried out by heating PA6/NPPMS

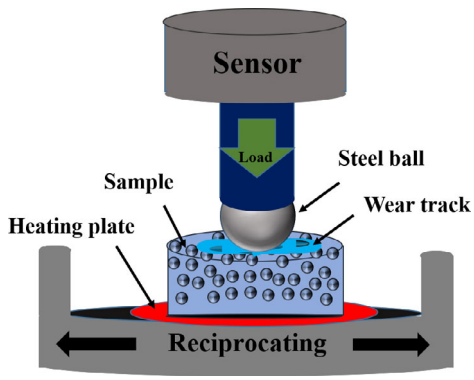

Fig. 3 Schematic diagram of a testing system for tribological performance.

composites on the bottom heating plate. The COF was automatically recorded with a friction and wear tester, the wear volume (v) of the specimens was measured by a confocal microscope (Anton Paar, Conscan). Finally, the wear rate (ε) was calculated using Eq. (1) [5]:

$$\varepsilon = v / (F \cdot L) \tag{1}$$

where F is the applied normal load (N) and L is total sliding distance (m). To minimize experimental errors, all friction tests were conducted in air three times for test reproducibility.

3 Results and discussion

3.1 Morphological analysis of NPPMS and PA6/NPPMS composites

Figure 4(a) shows the SEM image of PSF/PAO40 microcapsules with a smooth surface.

The particle size is mostly between 20 and 60 μm, which has been reported in our previous study [5]. After electroless nickel plating, microcapsules surfaces become rough in possession of a metallic luster (Fig. 4(b)). Furthermore, the removal of organic matter in NPPMS was achieved by means of the calcination at 550 °C for 3 h in order to obtain surface nickel shells. The Ni shell obtained has wrinkles and partial collapse (Fig. 4(c)), because Ni is a very thin layer on the PSF, when the PSF is decomposed, the thin Ni layer will lose the support and cause deformation. The cross-sectional morphology and EDS analytical results were demonstrated in Figs. 4(d) and 4(e), respectively. It has been observed that NPPMS is completely embedded in PA6 matrices. The part of Ni layer is peeled off along with PA6 matrices, which may suggest the excellent interfacial bonding between rough Ni layer and PA6 matrices. As illustrated in Fig. 4(f), the XRD pattern of NPPMS appears to be similar to the standard diffraction peak of neat Ni [31], further confirming the existence of Ni as the coating material generated on PSF/PAO40 microcapsules.

3.2 Thermal stability of NPPMS

The weight losses of PSF/PAO40 microcapsules and NPPMS due to the thermal effect are caused by the decomposition of PAO40 as the core material, whose phenomenon started from approximately 350 °C. Between 470 and 500 °C, TGA curves of PSF/PAO40 microcapsules and NPMMS remain stable, signifying that PAO40 is completely decomposed at 470 °C. At the same time, it can be demonstrated from the decomposition process of PAO40 that the loading capacities of PSF/PAO40 microcapsules and NPPMS both reach about 50%. The core material contents of PSF/PAO40 microcapsules and NPPMS are basically

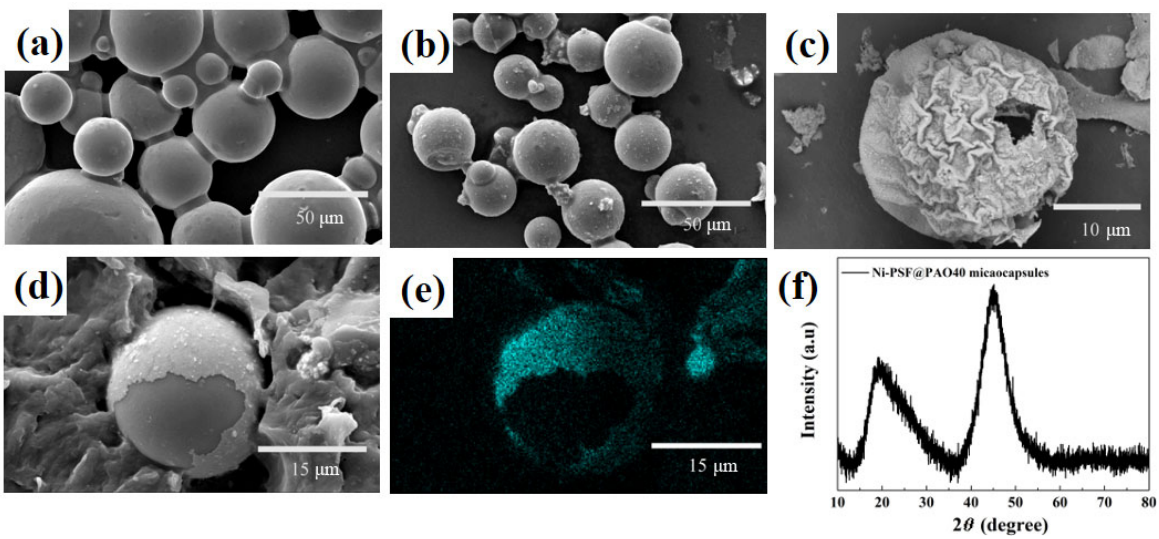

Fig. 4 SEM images for different materials of interest: (a) PSF/PAO40 microcapsules, (b) NPPMS, (c) residual Ni shells after the calcination of NPPMS, (d) cross-sectional morphology of PA6/NPPMS composites, (e) corresponding distribution of element Ni in the cross-section, as well as (f) XRD patterns of NPPMS.

the same, which implies that PSF/PAO40 microcapsules were not damaged and the core material was not lost during the process of electroless nickel plating. After the end of weight loss, the remaining mass of NPPMS is higher than that of PSF/PAO40 microcapsules, which is attributed to high-temperature resistant Ni existing in NPPMS.

In order to investigate macroscopic heat resistance, PSF/PAO40 microcapsules and NPMMS were heated in a vacuum heating furnace at 200, 300, and 400 °C, as well as held for 30 minutes, respectively. At 30 °C, PSF/PAO40 microcapsules and NPPMS are white and black powders at a macroscopic level (Figs. 6(a_1) and Fig. 6(e_1)), and they both appear to be regular spheres at the microscopic level instead (Figs. 6(a_2) and 6(e_2)). When the temperatures increase to 200, 300, and 400 °C, PSF/PAO40 microcapsules tend to dissolve together, and as a result, they appear to be in form of yellow liquid, brown liquid, and black liquid (Figs. 6(b_1), 6(c_1), and 6(d_1)), respectively. On the contrary, NPPMS still remain black powders (Figs. 6(f_1), 6(g_1), and 6(h_1)). At the microscopic level, PSF/PAO40 microcapsules can no longer become spherical particles (Figs. 6(b_2), 6(c_2), and 6(d_2)), but NPPMS still appear to be regular spherical microcapsules (Figs. 6(f_2), 6(g_2), and 6(h_2)). However, after reaching 300 °C, micropores will appear on the surface of NPPMS, which are caused by the gas generated by the decomposition of PAO40 to break through the weak part of the shells.

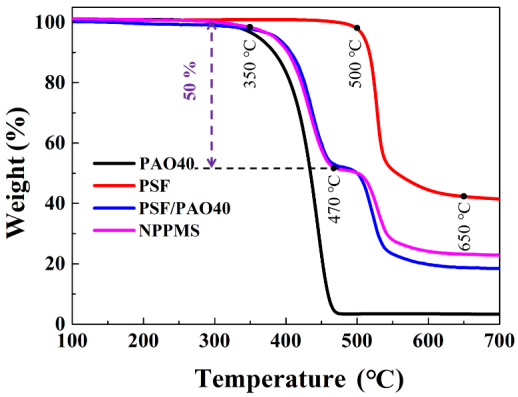

Fig. 5 TGA curves of PAO40, PSF, PSF/PAO40 microcapsules and NPPMS.

3.3 Stability of NPPMS in organic solvents

The application of microcapsules as the additives often involves blending or combining with other

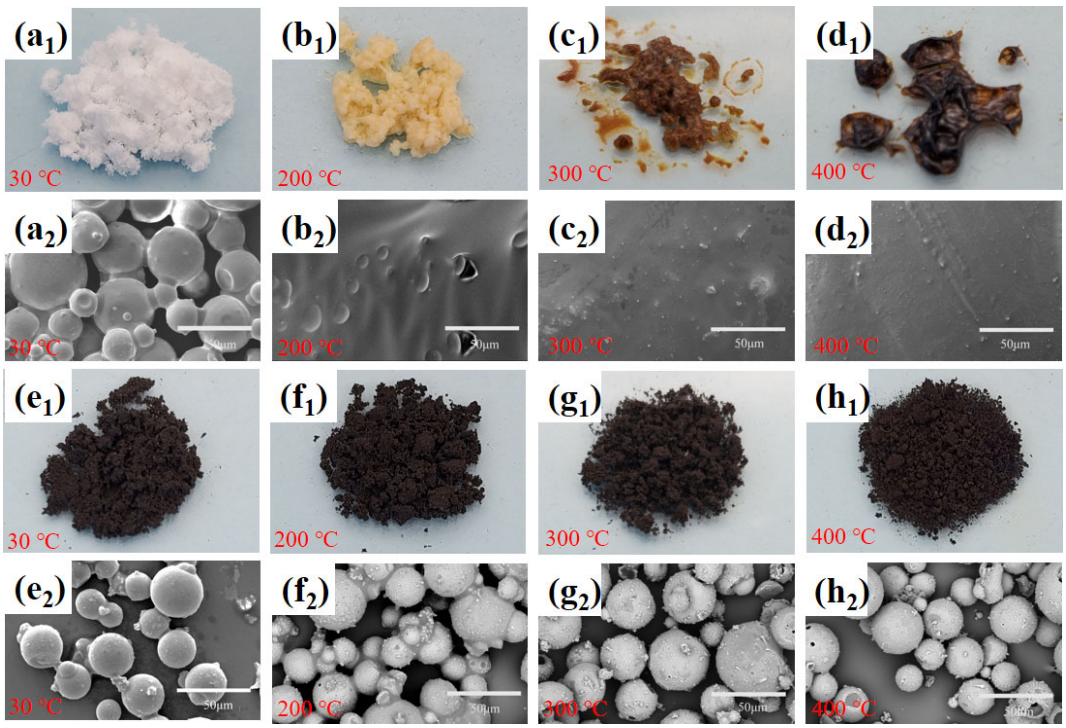

Fig. 6 Macroscopic morphologies of PSF/PAO40 microcapsules at different temperatures: (a_1) 30 °C, (b_1) 200 °C, (c_1) 300 °C, (d_1) 400 °C, and (a_2)–(d_2) are their microscopic morphologies. Macroscopic morphologies of NPPMS at different temperatures: (e_1) 30 °C, (f_1) 200 °C, (g_1) 300 °C, (h_1) 400 °C, and (e_2)–(f_2) are their microscopic morphologies.

materials in organic solvents. Therefore, some typical organic solvents were chosen in this study including low-polar petroleum ether, medium polar ethyl acetate, and polar acetone as the solvents to evaluate the chemical stability of PSF/PAO40 microcapsules and NPPMS. The specific tests were performed by immersing PSF/PAO40 microcapsules and NPPMS in organic solvents for 7 days in order to examine their surface morphologies by SEM. In petroleum ether, there is no obvious change in the morphologies of PSF/PAO40 microcapsules and NPPMS (Figs. 7(a_1) and 7(a_2)). However, the surfaces of PSF/PAO40 microcapsules are wrinkled and a part of them are broken in ethyl acetate despite no change identified for NPPMS (Figs. 7(b_1) and 7(b_2)). In acetone, the surface of PSF/PAO40 microcapsules becomes uneven, and NPPMS still maintain its original shape. Therefore, NPPMS have excellent stability in organic solvents. This is associated with the high stability of dense Ni layer on the surface to isolate the internal organic matter from the organic solvent.

3.4 Mechanical properties of PA6/NPPMS composites

Figure 8(a) shows typical nanoindentation curves of neat PA6 and PA6/NPPMS composites. Under the same loads (F_n), the indentation depths of all PA6/NPPMS composites were smaller than that of neat PA6, indicating an increase in the microhardness of PA6/NPPMS composites. Figure 8(b) reveals the relationship between the microhardness and NPPMS content. It can be seen that the microhardness of PA6/NPPMS composites was enhanced with increasing the NPPMS content. When NPPMS content is 20 wt%, the microhardness of PA6/NPPMS composites was about 19% greater than that of neat PA6. Such results are expected because the incorporation of hard particles usually enhances the hardness of polymer matrices [36–38]. Figure 8(c) shows typical compressive stress-strain curves of PA6 and PA6/NPPMS composites. Under the same compressive stress, the deformations of PA6/NPPMS composites were larger than that of neat PA6. As the NPPMS content increased, the compressive strength of PA6/NPPMS composites decreased. When the NPPMS content is 20 wt%, the compressive performance of PA6/NPPMS composites decreases significantly. This is because NPPMS contains liquid lubricants, which can generate local defects in PA6 matrices. The local defects yield a decrease in the compression performance of PA6/NPPMS composites [4, 39].

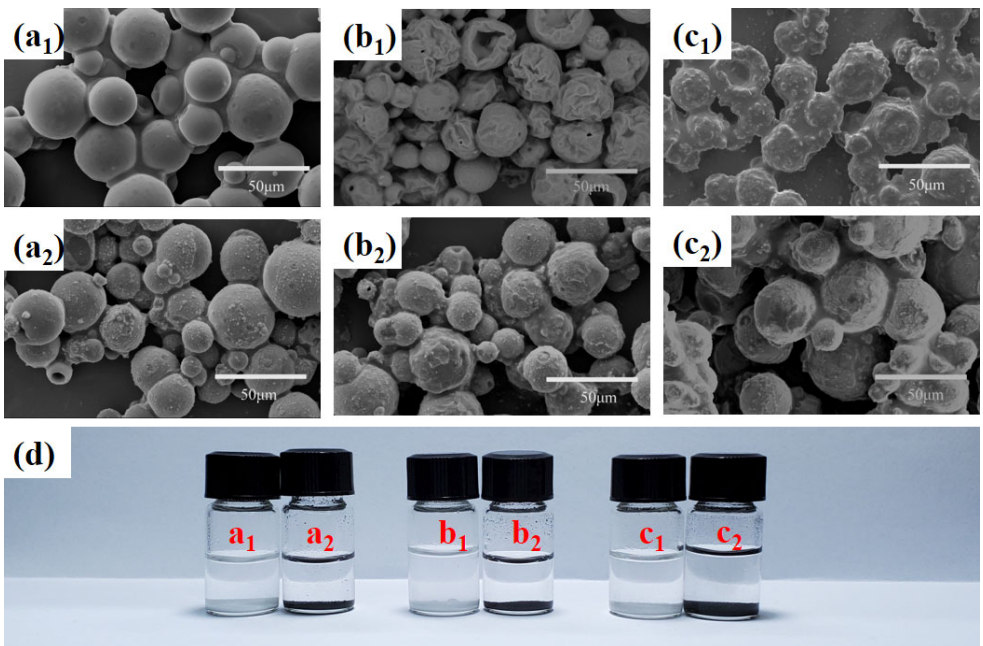

Fig. 7 Macroscopic morphologies of PSF/PAO40 microcapsules and NPPMS after immersion in some typical organic solvents for 7 days: petroleum ether ((a_1) PSF/PAO40 microcapsules, (a_2) NPPMS); ethyl acetate ((b_1) PSF/PAO40 microcapsules, (b_2) NPPMS); acetone ((c_1) PSF/PAO40 microcapsules, (c_2) NPPMS), (d) photographs of tested samples.

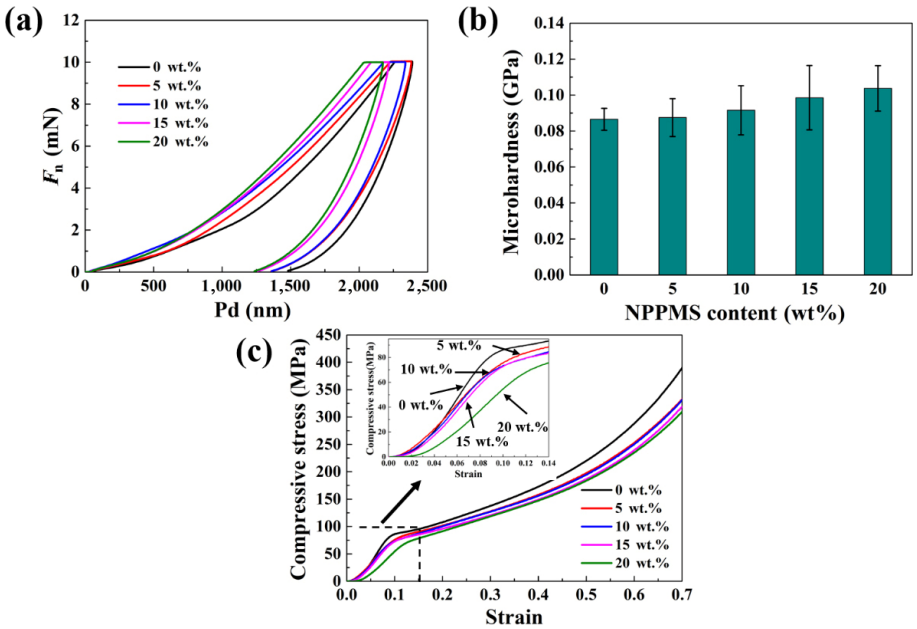

Fig. 8 Mechanical properties of neat PA6 and PA6/NPPMS composites: (a) nanoindentation curves, (b) microhardness, and (c) typical compressive stress–strain curves.

3.5 Lubrication performance of NPPMS in PA6

Firstly, the external lubrication effect of PAO40 was confirmed. PAO40 at room temperature and after 260 °C treatment was added to the friction interface of neat PA6, respectively. As shown in Fig. 9(a), the COF of neat PA6 was reduced from 0.5 to 0.03 after adding 2.5 μL PAO40 into the friction interface. In particular, there is no evident effect on the lubricity of PAO40 after heating up to 260 °C. Figure 9(b) presents the relationship between the COF of PA6/NPPMS composites and NPPMS content at the load of 10 N and the reciprocating frequency of 1.5 Hz. The COF of neat PA6 gradually increased from relatively low 0.35 to 0.49 over time. After the incorporation of NPPMS, the tribological properties of PA6/NPPMS composites were found to be greatly improved. When NPPMS content was 10 wt%, the lowest COF of PA6/NPPMS composites was 0.06. With increasing the NPPMS content, the lubricating properties of NPPMS in PA6 matrices gradually decreased. As for PA6/NPPMS composites with 20 wt% NPPMS, the COF increased from the lowest at 0.06 to 0.1. It is inferred that an appropriate amount of NPPMS had an excellent lubricating effect on PA6 matrices, which is because NPPMS ruptured during the friction process and released PAO40 to form lubricating films at the friction interface [20, 26–28]. Nevertheless, excessive NPPMS might agglomerate in PA6 matrices, and poor dispersion affects the lubrication effect of NPMMS, thus resulting in a slight increase in the COF [4]. Furthermore, the lubrication properties of PA6/NPPMS composites with 10 wt% NPPMS were further investigated at different loads and sliding speeds. As shown in Fig. 9(c), when the load was 10 N, as the sliding speeds increased, the COF increased gradually. When the reciprocating frequency was 3 Hz, as the applied loads increased, the COF decreased gradually, the squeezing effect on NPPMS became greater and more PAO40 was released to the friction interface. This phenomenon was conducive to the formation of a continuous and stable lubricating oil film. The effect of experimental temperatures on the lubrication of PA6/NPPMS composites with 10 wt% NPPMS was investigated under the applied load of 10 N and the reciprocating frequency of 3 Hz. As shown in Fig. 9(d), with increasing experimental temperatures, the COF of PA6/NPPMS composites more rapidly reached a stable state, and the stable COF was lower than that at room temperature. The temperature increase resulted in the decrease of adhesion and the increase in fluidity for PAO40, which made it easier to achieve good lubrication at the friction interface.

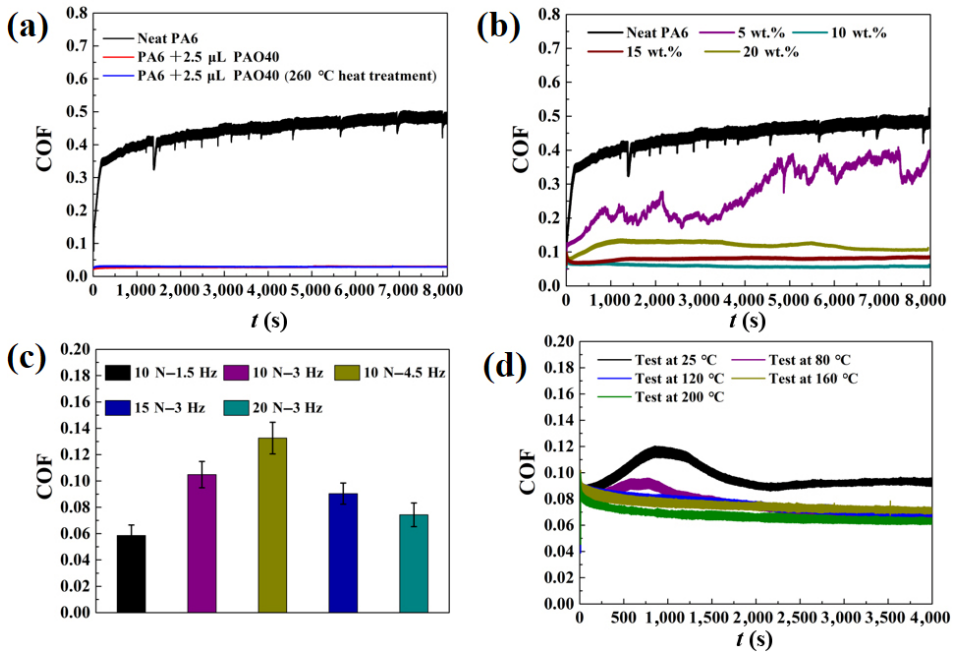

Fig. 9 Frictional properties of pure PA6 and PA6/NPPMS composites: (a) COFs of near PA6, PA6 + 2.5 μL PA040, and PA6 + 2.5 μL PA040 (after heating at 260 °C) under 1.5 Hz and 10 N, (b) COFs of neat PA6, PA6/NPPMS composites with different NPPMS contents (i.e., 5, 10, 15, and 20 wt%) under 1.5 Hz and 10 N, (c) average COFs of PA6/NPPMS composites with 10 wt% NPPMS at different loads and sliding speeds, (d) COFs of PA6/NPPMS composites with 10 wt% NPPMS at different test temperatures.

Figure 10 shows corresponding 2D images, section images, and 3D topographies of wear tracks on neat PA6 and PA6/NPPMS composites, respectively. With the addition of NPPMS, the wear track widths (Figs. 10(a_1)–10(e_1)) and depths (Figs. 10(a_2)–10(e_2)) of PA6/NPPMS composites have been greatly reduced. Among them, PA6/NPPMS composites with 10 wt% NPPMS yielded the lowest wear width and depth. The 3D images demonstrate that the wear track of neat PA6 is rough and uneven (Fig. 10(a_3)). With the addition of NPPMS, the wear tracks become more smoother than that of neat PA6 (Figs. 10(a_3)–10(e_3)), which indicates that NPPMS enable to optimize the wear form on the friction interface.

To investigate the wear tracks in detail, Fig. 11 shows the SEM images of wear tracks on neat PA6 and PA6/NPPMS composites, respectively. Neat PA6 shows severe wear that can be characterized by large-area peeling on the wear track. After adding 5 wt% of NPPMS, the wear track becomes smooth with only a small amount of slight peels. When NPPMS contents reach 10 wt% and 15 wt%, the wear tracks become smoother, which shows that suitable NPPMS can make good lubricating effect. When NPPMS content further increases up to 20 wt%, it can be clearly seen that NPPMS agglomerate (NPPMS agglomeration phenomenon shown in Fig. S1 in the Electronic Supplementary Material (ESM)), as well as poor dispersibility results in inefficient lubrication of NPPMS in the friction process [4]. In addition, broken NPPMS can be seen in the wear tracks of PA6/NPPMS composites (Figs. 11(b)–11(e)). Subsequently, broken NPPMS cavities collect the wear debris falling from PA6 matrices, which can reduce the secondary damage to the friction interface caused by the wear debris.

Figure 12 shows the wear rates and surface roughness of neat PA6 and PA6/NPPMS composites at different NPPMS contents. As shown in topographic images (Fig. 10) and SEM images (Fig. 11) for the wear tracks, the addition of NPPMS greatly reduces the wear of PA6 and improves the smoothness of wear tracks. The wear rate and surface roughness of neat PA6 are 1.29×10^{-5} mm^3/(N·m) and 5,076 nm, respectively. After adding 10% NPPMS, the wear rate and surface roughness appear to be 4.15×10^{-7} mm^3/(N·m) and 110 nm accordingly, which are 96.8% and 97.8% lower than that of neat PA6. As expected, low surface roughness is beneficial to achieve a good lubrication state.

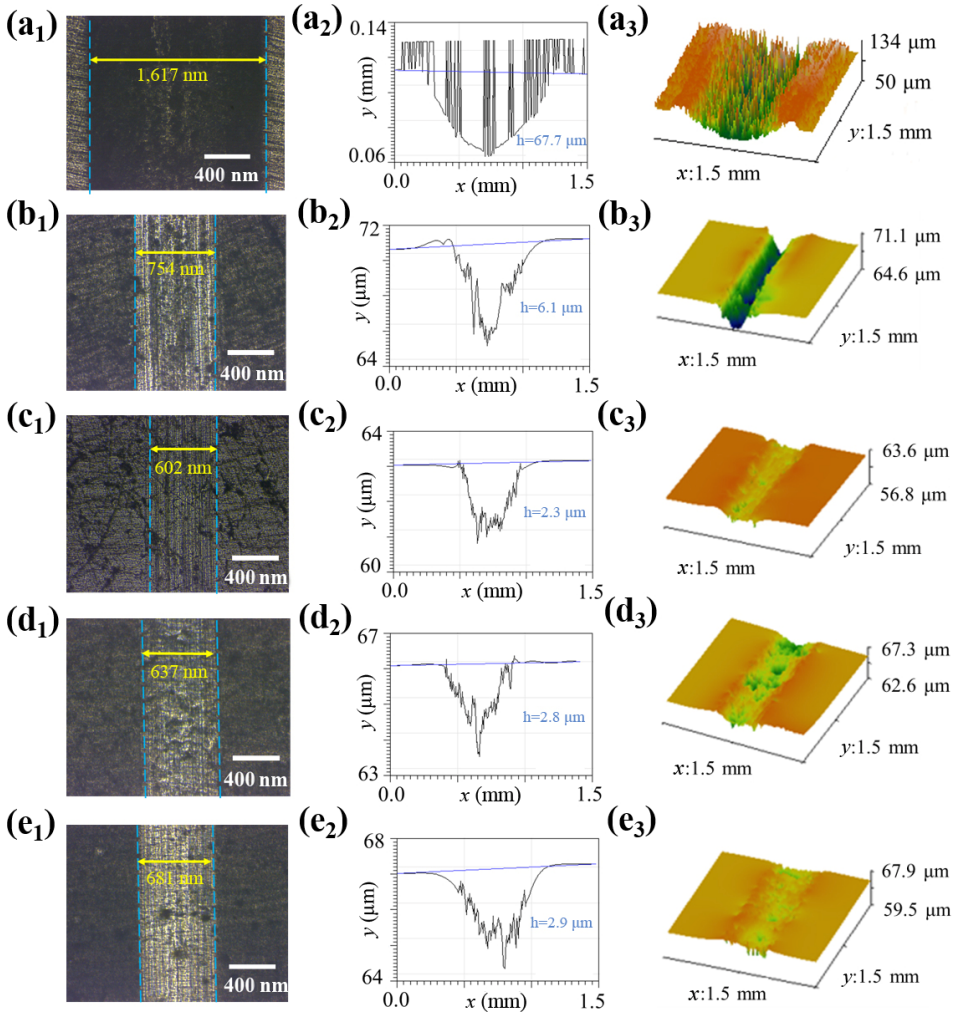

Fig. 10 Topographic images of wear tracks on neat PA6 and PA6/NPPMS composites. 2D images: (a_1) neat PA6, (b_1) PA6 with 5 wt% NPPMS, (c_1) PA6 with 10 wt% NPPMS, (d_1) PA6 with 15 wt% NPPMS, (e_1) PA6 with 20 wt% NPPMS. (a_2)–(e_2) and (a_3)–(e_3) are their corresponding section images and 3D topographies, respectively.

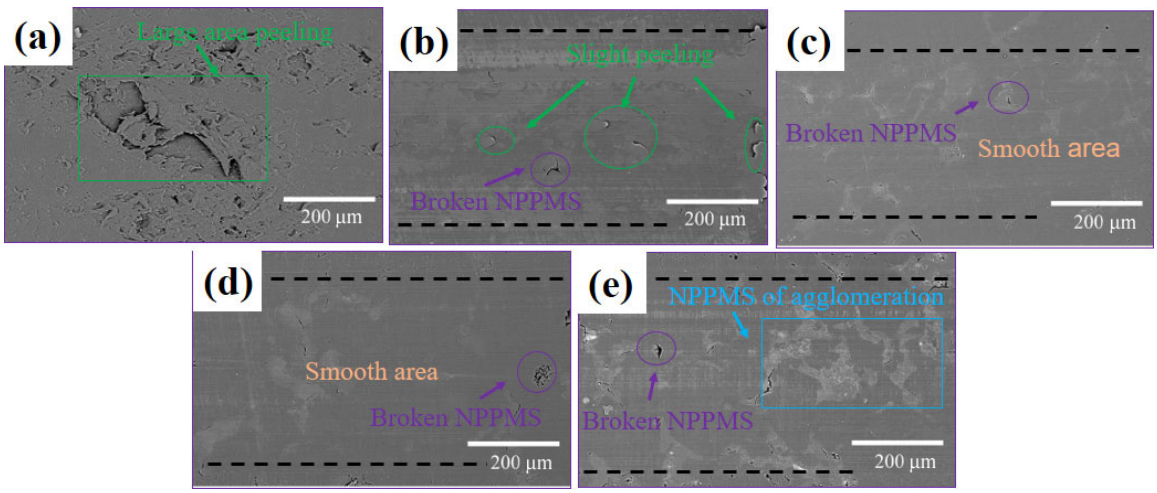

Fig. 11 SEM morphologies of wear tracks on neat PA6 and PA6/NPPMS composites: (a) neat PA6, (b) PA6/NPPMS composites with 5 wt% NPPMS, (c) PA6/NPPMS composites with 10 wt% NPPMS, (d) PA6/NPPMS composites with 15 wt% NPPMS, (e) PA6/NPPMS composites with 20 wt% NPPMS.

Figure 13 shows the surfaces of corresponding steel ball. With respect to neat PA6, a large amount of PA6 debris and obvious scratches have been observed on the steel ball surface (Fig. 13(a)). Combined with the wear track of neat PA6 (Fig. 11(a)), it can be inferred that the main wear forms of PA6 are fatigue and adhesive wears. Fatigue wear causes partial peeling of PA6, which leads to pits and uneven wear track. Scratches are caused by pit parts in the uneven wear track. The edge of the pit is equivalent to a sharp area. The small contact area between the pit edge and the steel ball causes the local pressure to increase, thereby scratching the steel ball. (Magnified SEM image of a steel ball scratched by PA6 is Fig. S2 in the ESM). With the addition of 5 wt% of NPPMS, the wear on the steel ball surface is significantly lighter, and the wear debris are distributed around the wear scar. (Fig. 13(b)). As shown in Fig. 13(c), when NPPMS content reaches 10 wt%, no obvious scratches and wear debris have been detected on the steel ball surface. This phenomenon indicates that the addition of suitable NPPMS can prevent the generation of large-area PA6 debris. PAO40 released by NPPMS can induce good lubrication effect on the friction interface in order to protect the steel ball. Nevertheless, when NPPMS content increases up to 20 wt%, some wear debris is attached to the surface of the steel ball again. This may be related to an excessive amount of NPPMS to cause a decrease in the mechanical properties of PA6 matrices, resulting in easy peeling in the friction process.

3.6 Anti-friction and anti-wear mechanisms

Figure 14(a) shows a typical SEM image of smooth wear track with NPPMS lubrication. Figure 14(b) shows an enlarged view of the broken NPPMS. In addition, Fig. 14(c) is the distribution diagram of S element in the wear track in Fig. 14(a), S element has

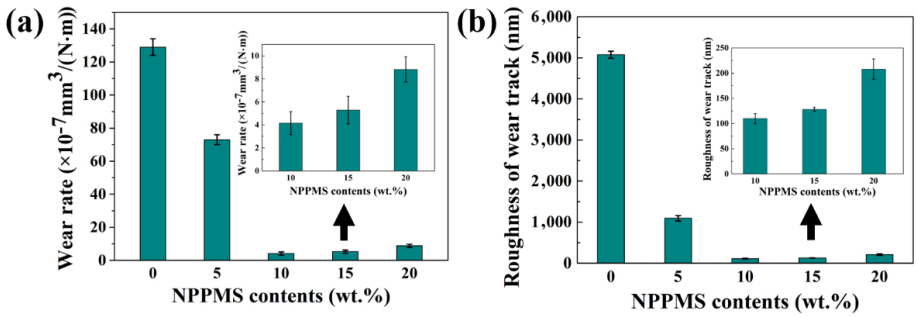

Fig. 12 (a) Wear rates of neat PA6 and PA6/NPPMS composites, (b) surface roughness of wear tracks.

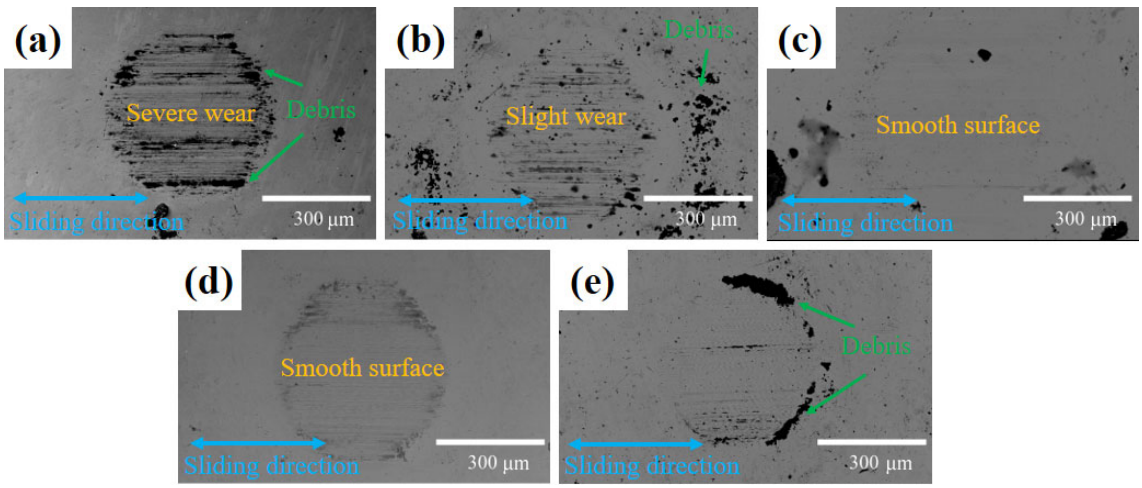

Fig. 13 SEM images of ball surfaces sliding against neat PA6 and PA6/NPPMS composites: (a) neat PA6, (b) PA6/NPPMS composites with 5 wt% NPPMS, (c) PA6/NPPMS composites with 10 wt% NPPMS, (d) PA6/NPPMS composites with 15 wt% NPPMS, (e) PA6/NPPMS composites with 20 wt% NPPMS.

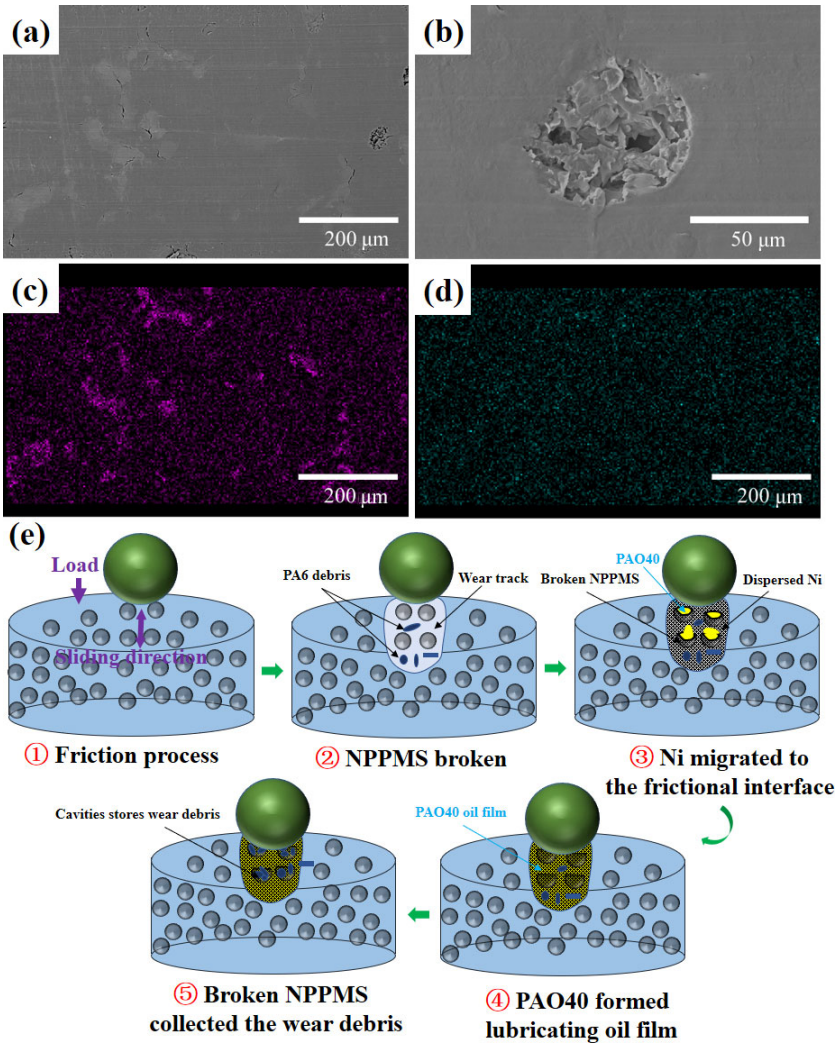

Fig. 14 Anti-friction and anti-wear mechanisms: (a) typical smooth wear track, (b) broken NPPMS, (c) distribution of the representative element S of NPPMS in the wear track, (d) distribution of element Ni in the wear track, (e) schematic diagram of NPPMS lubrication mechanism.

a local agglomeration phenomenon in the wear track. Apparently, S is a representative element of inner shell PSF in NPPMS, which can be used to locate the areas where the broken NPPMS is located. Figure 14(d) shows the distribution of Ni element in the wear track, which is evenly distributed throughout the wear track. It can be inferred that the lubrication mechanism of NPPMS is clearly revealed in Fig. 14(e). During the friction process, the brittle Ni shell outside NPPMS is broken, and the crushed metal Ni is carried into the entire wear track along with the sliding process, which improves the surface hardness of the wear track. The Ni-PA6 layer can prevent further peeling of PA6 matrices and improve the wear resistance of PA6/NPPMS composites. Furthermore, the ruptured NPPMS released PAO40 to the friction interface, which plays an important lubricating role accordingly. Finally, the remaining cavity of NPPMS can collect the wear debris generated by the matrices, which further enables to prevent secondary damage caused by the wear debris during the friction process.

4 Conclusions

A novel type of self-lubricating microcapsules (NPPMS) with high stability has been synthesized successfully by electroless nickel plating onto the surface of PSF/PAO40 microcapsules. When compared with conventional PSF/PAO40 microcapsules, the high-temperature resistance and chemical stability of

NPPMS have been significantly improved. Furthermore, NPPMS were added to PA6 matrices by vacuum hot press molding for the preparation of PA6/NPPMS composites in order to determine their mechanical properties and tribological properties. The microhardness of PA6/NPPMS composites has increased, which is caused by the incorporation of metallic Ni. On the contrary, the compressive strength has decreased because the liquid lubricant PAO40 in NPPMS forms local defects in PA6 matrices. The COF and the wear rate of PA6/NPPMS composites have been greatly reduced as opposed to those of neat PA6. When the NPPMS content is 10%, PA6/NPPMS composites achieve the best tribological performance, the COF could be reduced by 87.7% (from 0.49 to 0.06) and the wear rate could be diminished by 96.8% (from 1.29×10^{-5} to 4.15×10^{-7} $mm^3/(N\cdot m)$) as opposed to those of neat PA6. Further studies confirm that increasing the test loads and test temperatures would be beneficial to improve the lubrication performance of NPPMS despite the opposite results obtained when increasing the sliding speeds. Synthetic NPPMS have excellent thermal stability, resistance to organic solvents, and lubrication performance, which can be incorporated into many other polymers to yield self-lubricating composites with a remarkably high performance.

Declaration of competing interest

The authors declare that they have no known competing financial interests or personal relationships that could have appeared to influence the work reported in this paper.

Acknowledgements

This work was supported by the Doctoral Fund Project of Yanshan University (No. BL18057), Aviation Scientific Fund Project (No. 20200045099001), and Aviation Scientific Fund Project (No. 20184599001).

Electronic Supplementary Material: Supplementary material is available in the online version of this article at https://doi.org/10.1007/s40544-021-0560-y.

References

[1] Li X L, Wu S, Ling Y L, Zhang C H, Luo J B, Dai Y J. Preparation and tribological properties of PTFE/DE/ATF6 composites with self-contained solid-liquid synergetic lubricating performance. *Compos Commun* **22**: 100513 (2002)

[2] Li X L, Ling Y L, Zhang G L, Yin Y C, Dai Y J, Zhang C H, Luo J B. Preparation and tribological properties of solid-liquid synergetic self-lubricating PTFE/SiO_2/PAO6 composites. *Compos Part B*: *Eng* **196**: 108133 (2020)

[3] Zhang G L, Xie G X, Si L N, Wen S Z, Guo D. Ultralow friction self-lubricating nanocomposites with mesoporous metal-organic frameworks as smart nanocontainers for lubricants. *ACS Appl Mater Interfaces* **9**(43): 38146–38152 (2017)

[4] Zhang L, Xie G X, Wu S, Peng S G, Zhang X Q, Guo D, Wen S Z, Luo J B. Ultralow friction polymer composites incorporated with monodispersed oil microcapsules. *Friction* **9**(1): 29–40 (2021)

[5] Zhang W L, Qi X W, Li X L, Dong Y, Yao W G, Liang L, Zhang Y. Surface modification of polysulfone/PAO40 microcapsules via polydopamine to improve thermal stability and used to prepare polyamide 6-based self-lubricating composite. *Colloids Surf A*: *Physicochem Eng Aspects* **625**: 126906 (2021)

[6] Li H Y, Chen S J, Li Z K, Feng Y Y, Zhang M J. Preparation of PU/GO hybrid wall microcapsules and their self-lubricating properties for epoxy composites. *Colloids Surf A*: *Physicochem Eng Aspects* **596**: 124729 (2020)

[7] Salaün F, Devaux E, Bourbigot S, Rumeau P. Influence of process parameters on microcapsules loaded with *n*-hexadecane prepared by *in situ* polymerization. *Chem Eng J* **155**(1–2): 457–465 (2009)

[8] Gong H J, Song Y, Li G L, Xie G X, Luo J B. A highly tough and ultralow friction resin nanocomposite with crosslinkable polymer-encapsulated nanoparticles. *Compos Part B*: *Eng* **197**: 108157 (2020)

[9] Khun N W, Zhang H, Sun D W, Yang J L. Tribological behaviors of binary and ternary epoxy composites functionalized with different microcapsules and reinforced by short carbon fibers. *Wear* **350–351**: 89–98 (2016)

[10] Ma Y J, Li Z K, Wang H Y, Li H Y. Synthesis and optimization of polyurethane microcapsules containing [BMIm]PF_6 ionic liquid lubricant. *J Colloid Interf Sci* **534**: 469–479 (2019)

[11] Yang Z R, Guo Z W, Yuan C Q. Tribological behavior of polymer composites functionalized with various microcapsule core materials. *Wear* **426–427**: 853–861 (2019)

[12] Li H Y, Ma Y J, Li Z K, Ji J, Zhu Y J, Wang H Y. High temperature resistant polysulfone/silica double-wall microcapsules and their application in self-lubricating polypropylene. *RSC Adv* **7**(79): 50328–50335 (2017)

[13] Pang H B, Zhou S X, Wu L M, Chen M, Gu G X. Fabrication of silicone oil microcapsules with silica shell by miniemulsion method. *Colloids Surf A*: *Physicochem Eng Aspects* **364**(1–3): 42–48 (2010)

[14] Li H Y, Cui Y X, Wang H Y, Zhu Y J, Wang B H. Preparation and application of polysulfone microcapsules containing tung oil in self-healing and self-lubricating epoxy coating. *Colloids Surf A*: *Physicochem Eng Aspects* **518**: 181–187 (2017)

[15] Guo Q B, Lau K T, Rong M Z, Zhang M Q. Optimization of tribological and mechanical properties of epoxy through hybrid filling. *Wear* **269**(1–2): 13–20 (2010)

[16] Armada S, Schmid R, Equey S, Fagoaga I, Espallargas N. Liquid-solid self-lubricated coatings. *J Therm Spray Technol* **22**(1): 10–17 (2013)

[17] Zhang T, Zhang M, Tong X M, Chen F, Qiu J H. Optimal preparation and characterization of poly(urea-formaldehyde) microcapsules. *J Appl Polym Sci* **115**(4): 2162–2169 (2010)

[18] de la Paz Miguel M, Vallo C I. Influence of the emulsifying system to obtain linseed oil-filled microcapsules with a robust poly (melamine-formaldehyde)-based shell. *Prog Org Coat* **129**: 236–246 (2019)

[19] Zhang B Y, Zhang Z, Kapar S, Ataeian P, da Silva Bernardes J, Berry R, Zhao W, Zhou G F, Tam K C. Microencapsulation of phase change materials with polystyrene/cellulose nanocrystal hybrid shell via Pickering emulsion polymerization. *ACS Sustainable Chem Eng* **7**(21): 17756–17767 (2019)

[20] Li H Y, Ma Y J, Li Z K, Cui Y X, Wang H Y. Synthesis of novel multilayer composite microcapsules and their application in self-lubricating polymer composites. *Compos Sci Technol* **164**: 120–128 (2018)

[21] Wang H, Qi X W, Zhang W L, Dong Y, Fan B L, Zhang Y. Tribological properties of PTFE/Kevlar fabric composites under heavy loading. *Tribol Int* **151**: 106507 (2020)

[22] Karatas E, Gul O, Karsli N G, Yilmaz T. Synergetic effect of graphene nanoplatelet, carbon fiber and coupling agent addition on the tribological, mechanical and thermal properties of polyamide 6,6 composites. *Compos Part B*: *Eng* **163**: 730–739 (2019)

[23] Zhao Y L, Qi X W, Dong Y, Ma J, Zhang Q L, Song L Z, Yang Y L, Yang Q X. Mechanical, thermal and tribological properties of polyimide/nano-SiO_2 composites synthesized using an *in-situ* polymerization. *Tribol Int* **103**: 599–608 (2016)

[24] Costa M M, Bartolomeu F, Palmeiro J, Guimarães B, Alves N, Miranda G, Silva F S. Multi-material NiTi-PEEK hybrid cellular structures by Selective Laser Melting and Hot Pressing: Tribological characterization. *Tribol Int* **156**: 106830 (2021)

[25] Yan S C, Yang Y L, Song L Z, Qi X W, Zuo Z, Xue Y H. Tribological property of 3-aminopropyltriethoxysilane-graphite oxide nanosheets reinforced polyethersulfone composite under drying sliding condition. *Tribol Int* **103**: 316–330 (2016)

[26] Li H Y, Li S, Li Z K, Zhu Y J, Wang H Y. Polysulfone/SiO_2 hybrid shell microcapsules synthesized by the combination of Pickering emulsification and the solvent evaporation technique and their application in self-lubricating composites. *Langmuir* **33**(49): 14149–14155 (2017)

[27] Fujiwara M, Shiokawa K, Hayashi K, Morigaki K, Nakahara Y. Direct encapsulation of BSA and DNA into silica microcapsules (hollow spheres). *J Biomed Mater Res Part A* **81A**(1): 103–112 (2007)

[28] Yang Z X, Hollar J, He X D, Shi X M. A self-healing cementitious composite using oil core/silica gel shell microcapsules. *Cement Concrete Compos* **33**(4): 506–512 (2011)

[29] Sun D W, Zhang H, Zhang X, Yang J L. Robust metallic microcapsules: A direct path to new multifunctional materials. *ACS Appl Mater Interfaces* **11**(9): 9621–9628 (2019)

[30] Sun D W, Zheng Y, Lan M Z, Wang Z M, Cui S P, Yang J L. Robust and impermeable metal shell microcapsules

for one-component self-healing coatings. *Appl Surf Sci* **546**: 149114 (2021)

[31] Zhao W, Zhang Q Y, Chen T, Lu T L. Preparation and thermal decomposition of PS/Ni microspheres. *Mater Chem Phys* **113**(1): 428–434 (2009)

[32] Tsuneyoshi T, Ono T. Metal-coated microcapsules with tunable magnetic properties synthesized *via* electroless plating. *Mater Sci Eng B* **222**: 49–54 (2017)

[33] Mandal S, Sathish M, Saravanan G, Datta K K R, Ji Q M, Hill J P, Abe H, Honma I, Ariga K. Open-mouthed metallic microcapsules: Exploring performance improvements at agglomeration-free interiors. *J Am Chem Soc* **132**(41): 14415–14417 (2010)

[34] Du B Y, Cao Z, Li Z B, Mei A X, Zhang X H, Nie J J, Xu J T, Fan Z Q. One-pot preparation of hollow silica spheres by using thermosensitive poly(*N*-isopropylacrylamide) as a reversible template. *Langmuir* **25**(20): 12367–12373 (2009)

[35] Jeong U, Im S H, Camargo P H C, Kim J H, Xia Y N. Microscale fish bowls: A new class of latex particles with hollow interiors and engineered porous structures in their surfaces. *Langmuir* **23**(22): 10968–10975 (2007)

[36] Hui C, Yan F Y, Xue Q J, Liu W M. Investigation of tribological properties of Al_2O_3-polyimide nanocomposites. *Polym Test* **22**(8): 875–882 (2003)

[37] Ma J, Qi X W, Zhao Y L, Dong Y, Song L Z, Zhang Q L, Yang Y L. Polyimide/mesoporous silica nanocomposites: Characterization of mechanical and thermal properties and tribochemistry in dry sliding condition. *Mater Des* **108**: 538–550 (2016)

[38] Ji X L, Hampsey J E, Hu Q Y, He J B, Yang Z Z, Lu Y F. Mesoporous silica-reinforced polymer nanocomposites. *Chem Mater* **15**(19): 3656–3662 (2003)

[39] Behzadnasab M, Esfandeh M, Mirabedini S M, Zohuriaan-Mehr M J, Farnood R R. Preparation and characterization of linseed oil-filled urea–formaldehyde microcapsules and their effect on mechanical properties of an epoxy-based coating. *Colloids Surf A*: *Physicochem Eng Aspects* **457**: 16–26 (2014)

Wenli ZHANG. He received his bachelor degree in mechanical engineering in 2014 from Yanshan University, Qinhuangdao, China. Now, he is a Ph.D. student in the Key Laboratory of Fundamental Science for National Defense of Mechanical Structure and Materials Science under Extreme Conditions at Yanshan University. His research interests include core–shell materials, self-lubricating materials, and aviation self-lubricating motion pairs.

Xiaowen QI. He received his M.S. and Ph.D. degrees in mechanical engineering from Yanshan University, Qinhuangdao, China, in 2001 and 2009, respectively. He joined the Key Laboratory of Fundamental Science for National Defense of Mechanical Structure and Materials Science under Extreme Conditions at Yanshan University from 2007. His current position is a professor and the director of the laboratory. His research areas cover the tribology of self-lubricating composites, research and development of new self-lubricating materials and aviation self-lubricating motion pairs.

Bingli FAN. He received his M.S. and Ph.D. degrees in mechanical engineering from Yanshan University, Qinhuangdao, China, in 2007 and 2017, respectively. He joined the Key Laboratory of Fundamental Science for National Defense of Mechanical Structure and Materials Science under Extreme Conditions at Yanshan University from 2007. His current position is an associate researcher of the laboratory. His research areas cover the tribology of self-lubricating composites, research and development of new self-lubricating materials and aviation self-lubricating motion pairs.